THE ROYAL SOCIETY

Induced motion at texture-defined motion boundaries

Alan Johnston[1*], **Christopher P. Benton**[1] **and Peter W. McOwan**[1,2]

[1]*Department of Psychology, University College London, Gower Street, London WC1E 6BT, UK*
[2]*Department of Mathematical and Computational Sciences, Goldsmiths College, New Cross, London SE14 6NW, UK*

When a static textured background is covered and uncovered by a moving bar of the same mean luminance we can clearly see the motion of the bar. Texture-defined motion provides an example of a naturally occurring second-order motion. Second-order motion sequences defeat standard spatio-temporal energy models of motion perception. It has been proposed that second-order stimuli are analysed by separate systems, operating in parallel with luminance-defined motion processing, which incorporate identifiable pre-processing stages that make second-order patterns visible to standard techniques. However, the proposal of multiple paths to motion analysis remains controversial. Here we describe the behaviour of a model that recovers both luminance-defined and an important class of texture-defined motion. The model also accounts for the induced motion that is seen in some texture-defined motion sequences. We measured the perceived direction and speed of both the contrast envelope and induced motion in the case of a contrast modulation of static noise textures. Significantly, the model predicts the perceived speed of the induced motion seen at second-order texture boundaries. The induced motion investigated here appears distinct from classical induced effects resulting from motion contrast or the movement of a reference frame.

Keywords: computational model; motion; second order

1. INTRODUCTION

The motion of a spatial pattern is conveniently represented by a space–time plot in which the speed of motion is expressed as orientation (figure 1). The rigid motion of a spatial pattern can be detected by models which compute spatio-temporal energy (Adelson & Bergen 1985; Van Santen & Sperling 1985). Spatio-temporal energy models specify the construction of linear filters which are orientated in space–time. Even-symmetrical and odd-symmetrical filter outputs are combined by squaring and then adding to provide a measure of the match between the filter and the motion in a way which is insensitive to the spatial phase of the pattern (figure 1*a*). It is envisaged that this calculation is implemented by spatio-temporally orientated, cortical receptive fields (Adelson & Bergen 1985; Emerson *et al*. 1992). The filters used in the energy model are shown in figure 1*c*.

Second-order motion refers to a class of non-rigid movement defined by variation in some property other than luminance or colour, such as texture contrast (figure 1*b*). A significant feature of the second-order patterns investigated here is that they can be generated by the occlusion of one surface by another. Of particular interest are the motion signals generated at occluding boundaries where there is no overall change in the mean luminance at the boundary. The motion energy model cannot signal the correct direction of motion for these texture-defined and flicker-defined stimuli although motion is clearly seen (Chubb & Sperling 1988; Nowlan & Sejnowski 1994). Note that motion energy filters are sensitive to second-order patterns but the model does not deliver a consistent direction of motion (Benton & Johnston 1997). This has led to the proposal of additional mechanisms for dealing specifically with second-order motion sequences.

Although a number of varieties exist (Chubb & Sperling 1988; Cavanagh & Mather 1989; Werkhoven *et al*. 1993; Solomon & Sperling 1994; Wilson & Kim 1994; Zanker 1996; Clifford & Vaina 1999), the standard model for the second-order channel in multiple-motion mechanism theory employs an explicit nonlinear stage involving full-wave rectification or squaring. This stage is preceded by bandpass spatial or temporal filtering of the image which is often attributed to retinal mechanisms (Werkhoven *et al*. 1993). Bandpass filtering converts the distribution of light on the retina to a mean-zero signal which varies in sign and can thus be radically changed by a process such as rectification or squaring. The resulting signal can then be analysed by standard techniques. Typically, this might involve motion energy analysis (Adelson & Bergen 1985; Van Santen & Sperling 1985; Watson & Ahumada 1985) at a variety of spatial scales leading to a pattern of response across velocity-tuned detectors which is then interpreted as image motion (Heeger 1987; Wilson & Kim 1994; Simoncelli & Heeger 1998).

2. DO WE NEED A SPECIAL SECOND-ORDER CHANNEL TO SEE TEXTURE-DEFINED MOTION?

Although the question of whether there may be one, two, three or many separate channels for the analysis of motion has received much attention over the last decade

*Author for correspondence (a.johnston@ucl.ac.uk).

Received 15 July 1999 *Accepted* 20 August 1999

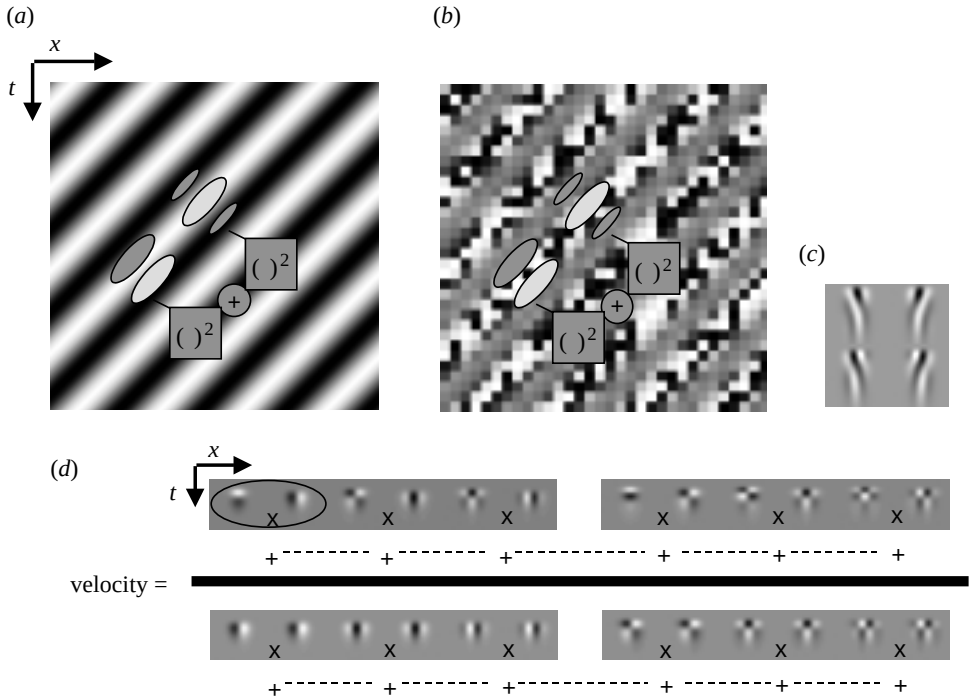

Figure 1. Second-order motion. (*a*) A space–time plot showing a moving grating with space–time-orientated filters superimposed. The motion energy model employs even and odd symmetrical space–time-orientated filters, the outputs of which are squared and added to provide a motion energy signal. The overlapping component filters have been separated for illustrative purposes. The motion energy filters are tuned to speed in a particular direction. (*b*) Contrast-modulated dynamic noise. A motion energy model does not signal a consistent direction of motion for this second-order pattern. (*c*) The space–time filters shown in (*a*) and (*b*) are highly schematic. Accurate renditions of pairs of space–time-orientated filters as described in Adelson & Bergen (1985) are shown here. (*d*) Some of the spatio-temporal differentiating filters and their pattern of connectivity as described in the Johnston & Clifford (1995*b*) gradient model. The sum of the products of the filter outputs on the numerator are divided by those shown on the denominator. Note the filter products on the numerator combine filters containing the same number of differential operations. The left filter of a pair (the first pair is circled) has one less spatial and one more temporal order of differentiation. Again all filters are applied at a single point in space–time.

(Derrington & Badcock 1985; Georgeson & Shackleton 1989; Cropper & Derrington 1994; Ledgeway & Smith 1994; Johnston & Clifford 1995*a*; Lu & Sperling 1995*a*,*b*; Nishida & Sato 1995; Smith & Scott-Samuel 1998), the proposal of multiple-motion mechanisms remains controversial. Much of the multiple-motion mechanism debate rests on the assumption that it is impossible to recover the motion of second-order variation without an implicit nonlinearity in the transduction of the image or an explicit nonlinear stage which introduces an equivalent luminance nonlinearity. It is this assumption which we wish to challenge.

We analysed the motion of a number of second-order motion sequences using a biologically plausible motion model which has recently been shown to compute the velocity of first-order patterns robustly in the presence of static noise (Johnston *et al*. 1999). Figure 1*d* shows some of the spatio-temporal filters used in the model and how they are combined. The mathematical details of the full implementation of the model are described elsewhere (Johnston *et al*. 1992, 1999; Johnston & Clifford 1995*a*). Velocity computation is based on the spatio-temporal gradient scheme in which the temporal derivative of image brightness is divided by the spatial derivative of image brightness. A model based solely on first derivatives is ill-conditioned at the peaks and troughs of image brightness where the spatial derivative is zero. We therefore combined the outputs of higher-order spatial derivative operators (figure 1*d*) in a way that only gives a zero denominator when all higher spatial derivatives are zero. This will only occur when the image is of uniform brightness. In this case the numerator is also zero and the velocity is indeterminate. We also included a set of filters which compute motion using first- and second-order temporal differentiating filters. One can think of these additional filters as computing the velocity of a temporally differentiated version of the input image. In order to compute speed and direction, speed estimates taken in many directions about an image point were combined (Johnston *et al*. 1999). An important aspect of this architecture is that the direction of motion is indicated by the sign of the product of pairs of differentiating filters, one of which computes one less spatial derivative and one more temporal derivative than its partner (circled in figure 1*d*).

3. COMPUTING DIRECTION IN TEXTURE-DEFINED AND FLICKER-DEFINED MOTION SEQUENCES

We have previously demonstrated that a gradient model can predict the perceived speed of motion of envelopes which modulate the contrast of a sine-wave grating

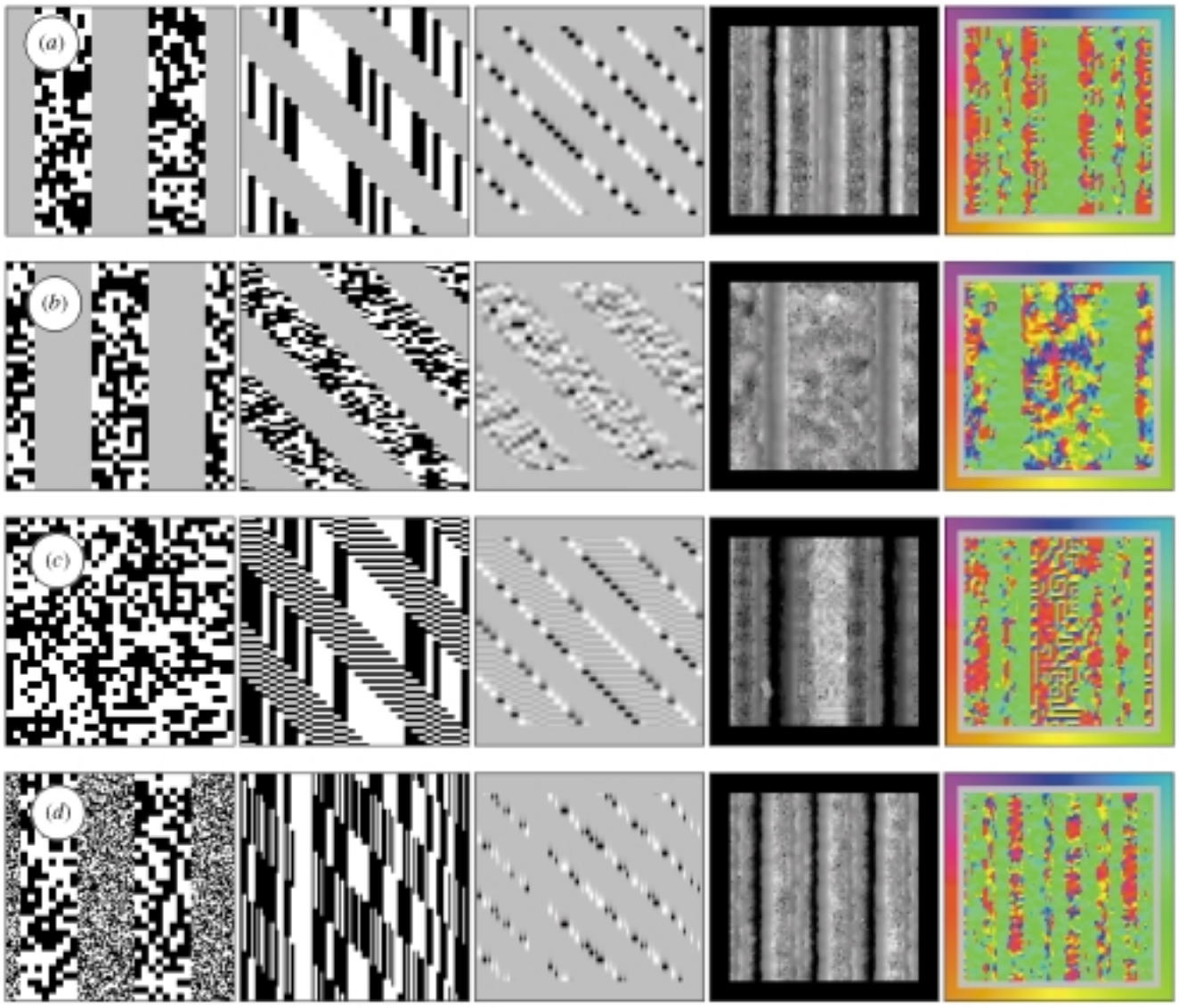

Figure 2. Single frame results for second-order motion sequences. Dense speed and direction images computed for arbitrarily chosen frames from second-order motion sequences. Column 1 shows single frames, column 2 shows space–time plots (time increasing downwards), column 3 shows the temporal derivative of the space–time plot, column 4 shows log speed maps (scaled to full brightness range, with black border set to a speed of zero) and column 5 shows the corresponding direction maps (direction coded by colour which should be read with reference to the colour border). All cases show square-wave modulations. (*a*) Contrast modulation of static binary noise. The envelope is moving rightwards (two cycles per image and two cycles per sequence: one sequence = 128 frames = 1 s, 128 pixels = 1° (Johnston & Clifford 1995*b*), image size = 128 × 128 and noise element size = 4 pixel × 4 pixel). (*b*) Contrast modulation of dynamic binary noise (parameters as in (*a*), with noise updated every two frames). (*c*) Modulation of temporal frequency, with maximum update rate once every two frames. (*d*) Modulation of spatial frequency, with maximum noise element size of 4 pixel × 4 pixel and minimum element size of 1 pixel × 1 pixel.

(Johnston & Clifford 1995*a*). Although second order, these sequences are not microbalanced (Chubb & Sperling 1988). Microbalanced second-order stimuli must conform to the stricter criterion of having equal motion energy in opposite directions for any windowed region of the stimulus. Typically, these stimuli involve modulations of a two-dimensional (2D) noise carrier. Our earlier model was designed to compute the speed and direction of motion of one-dimensional stimuli. It is not safe to assume that all types of second-order motion are processed by the same mechanism or that a mechanism that can detect one class of second-order motion can detect other classes without further proof. Our current model allows us to test whether the motion of 2D texture-defined and flicker-defined patterns require analysis by special mechanisms. The presence of sharp luminance discontinuities and dynamic motion noise in microbalanced second-order stimuli add considerably to the difficulty of detecting motion using a model based on spatio-temporal differentiation.

Figure 2 shows the results of applying the model to microbalanced second-order patterns defined by square-wave modulations of the contrast, temporal frequency and spatial frequency of either static or dynamic binary noise. For display purposes we show the logarithm of the speed in column 4 because dynamic carriers can produce large, isolated, transient spikes which mask the more typical values. The direction of motion is indicated in column 5 by colour which should be interpreted with reference to the surrounding coloured border. The modulation is moving

rightwards and so should appear as green. In each case there are areas showing a clear rightward motion signal. The multicoloured bands in figure 2*b* reflect the fact that dynamic noise contains additional local motion noise in high contrast regions. It is important to note that the modulation signal is present everywhere in each of these displays and could be recovered at all points by linear filtering followed by rectification. However, observers see a clear spatial variation of the motion signal. For the stimulus in figure 2*b*, observers reported smooth rightward motion in the low contrast regions and random motion noise in the high contrast regions. The stimulus in figure 2*c* appears as a flickering rightward moving pattern and the spatial frequency-modulated stimulus appears to move relatively smoothly rightwards. Although results for only one frame are shown in each case we analysed velocity distributions for many instantiations of the motion sequences which confirmed that the findings shown in figure 2 are typical. In each case we calculated a direction index (the total rightwards motion minus the total leftwards motion over the sum of these two; see § 6(a)) which gave values of 0.63 (figure 2*a*), 0.30 (figure 2*b*), 0.12 (figure 2*c*) and 0.54 (figure 2*d*).

The simulations demonstrate that it is possible to recover the direction of motion of microbalanced second-order motion without the introduction of pointwise early nonlinearities. Note that adopting a single channel model with a pointwise nonlinearity does not circumvent the second-order problem since, for stimuli such as those in figure 2*a*,*b*, it is always possible to find a grey luminance value which matches the mean level of the transformed texture. The spatial variations in velocity provide a better account of our perceptual experience than models which could explicitly recover the motion of the modulation at all points in space–time. For example, in figure 2*a* the model indicates rightward motion (green) in the envelope direction within the low and high contrast regions of the pattern and induced motion (red) close to the edges of the square-wave modulation. This is not predicted by models which rely on nonlinearities to explain the perception of texture-defined motion. To the extent that any nonlinearity exists (Badcock & Derrington 1989) the direction of motion of the resulting variation in the mean level will follow the envelope motion. To allow a quantitative comparison of these effects we measured the perceived speed of the envelope motion and the induced motion and plotted these data against the model predictions.

4. PERCEIVED SPEED OF TEXTURE-DEFINED MOTION AND INDUCED MOTION

Ledgeway and Smith (1995) showed that sine-wave contrast modulations of binary noise textures appeared to move at the same speed as comparable luminance-defined stimuli which were matched for visibility. We first replicated Ledgeway and Smith's (1995) experiment using our display. As a more stringent test of the model we investigated whether it was possible to predict the perceived speed of the induced effect. Because we found it was difficult to attend to the induced motion and a matching stimulus at the same time, we measured the induced effect by nulling with real motion. A method of constants (binary choice) psychophysical procedure was used to determine the carrier velocity required to null the induced motion.

(a) *Methods*

(i) *Psychophysics*

An adaptive method of the constants procedure (Watt & Andrews 1981) was used to estimate the point at which the velocity of a translating sine-wave grating with added static binary noise (first-order stimulus) matched the perceived envelope velocity (second-order stimulus). The second-order stimulus was a sinusoidal contrast modulation of static binary noise. For the first-order stimulus the contrast of the noise prior to the addition of the sine wave was 0.5. The mean contrast of the noise in the second-order stimulus was also 0.5. Subjects fixated a centrally placed cross which was removed during stimulus presentation. The stimulus pairs were presented sequentially in random order. The subjects indicated which of the two, the grating or the contrast envelope, appeared to move faster. The sequences were presented in a circular aperture (diameter = 5.31° and viewing distance = 1.5 m) with a Gaussian blurred edge (5 arcmin). The patterns were presented at five times their direction detection thresholds as measured for each subject by a method of adjustment. For both stimuli, the mean luminance was 28.3 cd m^{-2}, the noise element size was 7.4 arcmin^2 and the frame rate was 77 Hz. The spatial frequency of the sine wave was 1 c deg^{-1}. Each pattern was presented for 195 ms. Within each first-order–second-order pair the patterns were separated by a gap of 0.5 s. The minimum interstimulus interval between pairs was 5 s.

The speed of the apparent induced motion in the second-order pattern was measured by nulling with real carrier motion. In the nulling task a single second-order motion stimulus (modulation depth = 0.9, maximum contrast = 0.95 and minimum contrast = 0.05) was presented in each trial. The carrier speed and direction were varied from trial to trial. The subjects indicated the apparent direction of motion of the underlying noise carrier. The nulling speed was defined as the carrier speed at the 50% point on the psychometric function. Other stimulus parameters were identical to those used in the matching task.

(ii) *Modelling*

Full details of the model used in the simulations are given in Johnston *et al.* (1999). The filters are generated by differentiation of a single blur kernel defined by

$$K(r,t) = \frac{1}{4\pi\sigma} e^{-r^2/4\sigma} \frac{1}{\sqrt{\pi}\tau\alpha e^{\tau^2/4}} e^{-(\ln(t/\alpha)/\tau)^2}, \quad (1)$$

where $\sigma = 1.5$, $\alpha = 10$ and $\tau = 0.275$. The parameter t is time and r is the radial distance from the origin. These spatio-temporal parameters were set in previous work (Johnston & Clifford 1995*b*). The only other parameters are the highest order of spatial derivative used (6), the number of directions in which motion is computed (24) and the extent of an integration zone which defined the spatio-temporal support of local computations (11 pixel × 11 pixel × 11 pixel). These are identical to those used in previous work (Johnston *et al.* 1999). The square-wave

envelopes, which jumped in units of the largest block size to avoid introducing a local first-order motion within blocks, are shown in figure 2. The temporal update rate was chosen to deliver an envelope speed of 1 pixel per frame. The block size was 4 pixel × 4 pixel except in figure 2*d* where the smaller blocks were 1 pixel^2. The noise is updated every two frames within the dynamic region in figure 2*c*. The velocity distributions were based on ten instantiations of 64 frames of the model output for the simulations in figure 3. The modulation signal was shifted forward on every frame and resampled. The envelope spatial frequency was set at four cycles per image which was found to be optimal for accurate recovery of the envelope speed.

(b) ***Results***

We measured the response of the model to sinusoidal contrast modulations of a static binary noise texture as a function of modulation speed. The velocity field is much more variable for second-order than for first-order stimuli, so we plotted the distribution of responses (figure 3*a*), took a section through the distribution corresponding to the direction of stimulus motion (figure 3*b*) and then found the peak velocity. The modelling results are collated in figure 3*d*. The computed speed increased in direct proportion to the contrast envelope speed over the range of speeds tested. The predicted envelope speed is shown in figure 3*e* alongside psychophysical data for two subjects. The perceived speed increased linearly with the envelope speed as expected (Ledgeway & Smith 1995). The simulation results closely follow the psychophysical data. Data for three subjects are shown alongside the model predictions for the induced motion in figure 3*e*. The induced motion was approximately proportionate (18%, s.d. = 8.5) to the envelope speed. For the model, the induced speed was *ca.* 17% of the envelope speed. The model overestimates the induced effect somewhat at high envelope velocities.

5. ANALYSIS

The model of Johnston *et al.* (1999) is not designed to detect second-order motion; therefore, we need to consider what design features will deliver this emergent property. To explain how the model computes texture-defined motion we examined the sign of local spatio-temporal derivatives at texture boundaries. Like cortical receptive fields the filters in all local motion models sum their inputs over a spatio-temporal region. Because the gradient scheme specifies the computation of a ratio of filter outputs even small values can give rise to valid speed measures. Thus, a measure of image speed can be determined if there is some pattern that falls within the scope of the filter. In addition, the sign of the product of pairs of filters (circled, figure 1*d*), in which one takes one less spatial and one more temporal derivative than its partner, is dependent on the motion direction and insensitive to the sign of the spatial contrast (Johnston *et al.* 1992). This is a characteristic property of directionally selective cortical cells. These filter products signal the correct direction of envelope motion in the low contrast region of the contrast envelope (figure 4*a*,*b*), essentially because the signs of the changes over space and the changes over time are the same. The denominator is always positive. Although we used square-wave modulation in this analysis, the signs of the spatio-temporal derivatives are the same for sine-wave contrast modulation. The filter products in the high contrast region signal reversed motion (figure 4*c*). Since the pairs of filters on the numerator in figure 1*d* can be thought of as computing the first spatial and temporal derivatives of a spatially differentiated image, the analysis should apply to any pair of filters.

The same logic applies to filtering in the temporal domain. Filters like those on the right of figure 1*d*, which are temporally differentiated versions of the filters on the left of figure 1*d*, can be thought of as computing the speed of a temporally differentiated version of the input stimulus. This is because it does not matter whether differentiation is applied to the image or the filter—the outcome is the same. This explains the frequency doubling seen in figure 2*a*,*d*. Temporal differentiation of a square-wave texture contrast modulation generates a contrast-modulated pattern at twice the spatial frequency since there is no change in the centre of the grey and static high contrast regions. Change is signalled at the texture boundary. Hence, the final output of the model can be understood as a combination of the original and temporally differentiated signals, with envelope motion indicated in the high and low contrast regions and reversed motion at the texture boundaries. The influence of each of the filters on the final motion computation depends upon the magnitude of the filter outputs and their weights. Frequency doubling does not occur in figure 2*b*,*c* because there is dynamic change in either the occluding signal or the carrier. Temporal differentiation also allows the recovery of the temporal frequency-modulated stimulus (figure 2*c*).

6. TESTING THE LOCAL DERIVATIVE HYPOTHESIS

We propose that the induced motion seen in static binary texture carriers results from differential operations at texture boundaries. Induced effects are generally attributed to lateral interactions between motion detectors in adjacent regions (Nakayama & Loomis 1974) or frame effects (Dunker 1929). We varied the brightness level of the grey regions of a square-wave modulation of texture contrast (figure 5*a*). If the moving grey bars act as a reference frame against which a static pattern is seen to move, increasing the salience of the bars by making them brighter or darker than the mean luminance should enhance the induced effect. Similarly, increasing the luminance contrast of the inducing stimulus should enhance the motion contrast (Raymond & Darcangelo 1990; Nishida *et al.* 1997*a*). The prediction from the model is that the induced effect will get smaller when the uniform region is lighter or darker than the pixels making up the binary texture (figure 5*b*). A direction index of 1 indicates no induced motion. The amount of induced motion increases as the luminance of the grey bar approaches the mean luminance of the static binary texture. The shape of this function is essentially the same when the total amount of reversed motion is plotted against the luminance difference.

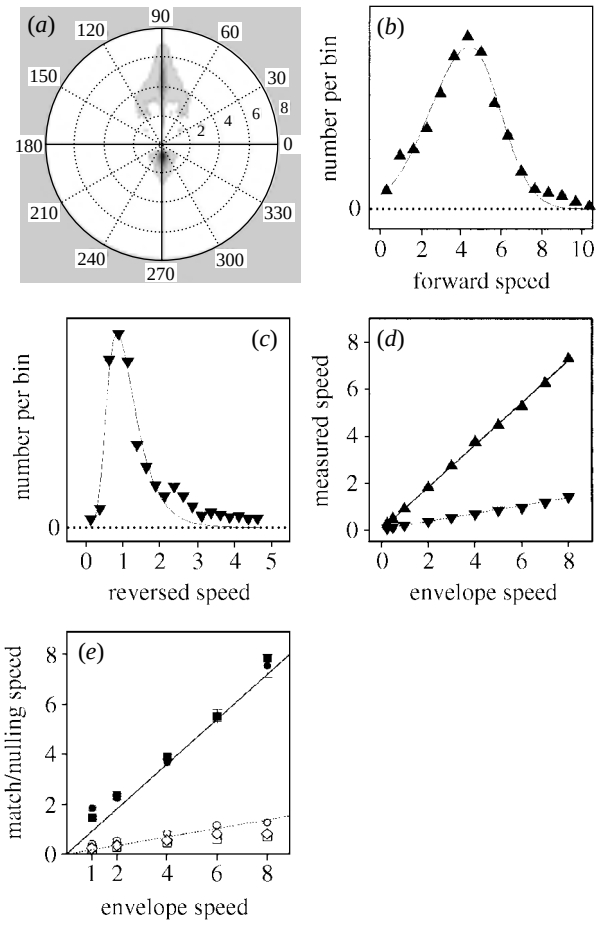

Figure 3. Model results for envelope and induced velocities. (*a*) Velocity distribution plot of output from the model in response to a translating sinusoidal contrast modulation of static binary noise with a velocity of $5^\circ\,s^{-1}$, a spatial frequency of $4\,c\,deg^{-1}$ (four cycles per image), a temporal frequency of 20 Hz (20 cycles per sequence) and a modulation depth of 1.0. (*b*) A slice through the velocity distribution taken in the direction of envelope motion showing a peak at $4.46^\circ\,s^{-1}$. (*c*) A slice through the velocity distribution in the direction opposite to the envelope motion showing a peak at $0.84^\circ\,s^{-1}$ for the induced motion. (*d*) Computed peak values for envelope (filled triangles) and induced (inverted filled triangles) motion over a range of envelope velocities. Slopes and correlations: envelope = 0.9 and $r = 0.999$ and induced motion = 0.17 and $r = 0.998$. (*e*) Psychophysical measurement of envelope and induced velocities. Filled symbols show the results of a speed matching task for subjects A.J. (squares) and C.B. (circles). Open symbols show the results for subjects A.J. (squares), C.B. (circles) and W.C. (diamonds) for a nulling task used to measure the perceived speed of the induced motion. Each data point represents the mean and standard error taken from six measures; each measure was derived from 64 presentations. The dotted line shows the prediction of the model for the perceived speed of envelope motion. The dashed line shows the prediction for induced motion velocity. In each case the speed axes are in degrees s^{-1}.

(a) *Method*

(i) *Psychophysics*

The nulling method was used to measure the induced motion seen in the static textured region as before. The spatial frequency of the square-wave modulation was set to $1\,c\,deg^{-1}$ (eight binary noise elements per cycle), the envelope velocity was $2^\circ\,s^{-1}$, the stimulus duration was 388ms (30 frames) and the contrast of the noise was set at 0.3. The uniform region was set to be a fixed ratio of the difference between the light and dark pixels and mean luminance, e.g. a value of 1 means the grey region is equal in brightness to the brightest pixel in the noise (figure 5*a*, left) and -1 matches the grey region with the darkest pixel (figure 5*a*, right). Note that changing the brightness of this region introduces first-order motion into the stimulus. Otherwise the methods were the same as those described above.

(ii) *Modelling*

The model was applied to square-wave contrast modulation of binary noise in which the luminance of the grey region was systematically varied. The texture block size was set at $4\,pixel \times 4\,pixels$, the modulation spatial frequency was four cycles per image and the envelope speed was two pixels per frame. The luminance of the uniform grey bars is expressed as multiples of the difference between the values of the brightest or darkest pixels in the texture and their mean. Model results were collected for 400 frames. The parameters of the model were not changed. Each frame was sampled from a separate randomly generated sequence. Since we observed that the main effect of changing bar luminance was a reduction in the amount of induced motion rather than a shift in the peak of the velocity distribution, we used a direction index to characterize the modelling results. A direction index was calculated from the velocity measures collapsed across frames and image points. The direction index was calculated as $S_x - S_{-x}/S_x + S_{-x}$, where S_x is the sum of the magnitude of the velocity components in the direction of envelope motion and S_{-x} is the sum of the magnitude of the velocity components in the opposite direction.

(b) *Results*

The psychophysical data are shown in figure 5*c*. Shifting the brightness level of the uniform region away from the mean luminance of the textured region reduced the induced motion in the static textured region. The induced effect is slightly less in the case of square-wave modulation and there is a slight bias in that the reduction is greater for the lighter bars.

There are a number of theoretically important implications of these data. The induced effect is greatest when the grey bar is at the mean luminance and the motion is second order. The reduction in the induced effect when the grey bar is shifted from the mean ensures that the induced effect is not due to luminance artefacts in the second-order pattern. In addition, the transformations in a hypothetical second-order channel, which make the contrast envelope explicit, deliver a spatially uniform motion signal. Thus, the induced effect cannot be intrinsic to a second-order channel. The possibility that activity in a second-order channel may induce motion in the static first-order carrier is unlikely since Nishida *et al.* (1997*a*) showed that flanking second-order motion does not induce movement in static gratings or static contrast-modulated noise. The multiple-mechanism theory's fundamental assumption is that the motion in the texture-defined case can only be seen by a

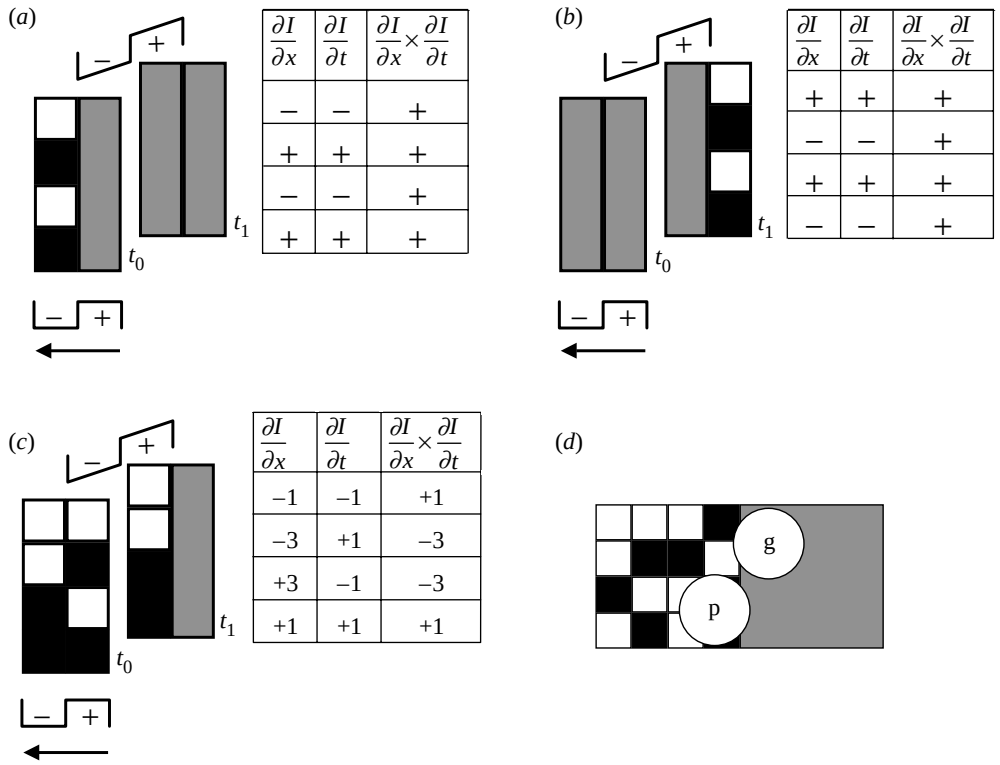

Figure 4. Motion signals at occluding boundaries. (*a*) The figure shows an eight pixel region at an occluding boundary for two consecutive frames t_0 and t_1. When a grey region (time t_1) occludes a pattern region (time t_0) analysis of the local differentials, using the approximations to differential operators $(-1, +1)$ shown $(-, +)$, demonstrates that the product of the spatial and temporal derivatives (as in the numerator of figure 1*d*) have the same sign irrespective of the sign of the spatial contrast at the boundary. The sign is calculated for each row by assigning the value 2 to a light bar, 1 to a grey bar and 0 to a dark bar. The temporal derivative is the sum of the first row of t_1 minus the sum of the first row of t_0, i.e. -1. The spatial derivative is calculated in an analogous way. (*b*) The same is true when the grey region moves on uncovering the image structure. (*c*) On the pattern side of the moving boundary, analysis of all possible combinations of the static pattern shows that there is a bias towards induced motion in the opposite direction to the motion of the grey bar. (*d*) In a ratio model even small filter values can serve to compute motion. A filter falling mainly on the grey region (g) of the second-order pattern will signal the direction of motion of the grey occluding surface, as in (*a*). A filter falling on the static patterned region (p) will indicate induced motion in the opposite direction, as in (*c*).

special second-order mechanism, but this viewpoint does not lead to an adequate explanation of the induced effect. We can conclude, with support from our simulations, that texture-defined motion is analysed by a luminance-based mechanism.

7. DISCUSSION

Albright (1992) described cells in the motion area (MT) which responded to luminance- and texture-defined motion as form-cue invariant. Form-cue invariance could result from the convergence of motion mechanisms specialized for different kinds of stimuli, although MT cell responses to first- and second-order stimuli are not equivalent (Albright 1992; O'Keefe & Movshon 1998). The simulations reported here demonstrate that form-cue invariance could be a consequence of robust strategies for motion encoding which allow analysis of a range of moving patterns rather than the convergence of specialized luminance- and texture-defined motion channels.

It is clear that it is possible to recover first-order motion and an important class of second-order motion with a single mechanism. More importantly, it is possible to predict the perceived speed of texture-defined motion and the speed and direction of motion of induced carrier motion. This is difficult to account for in multiple-mechanism theory because (i) models which rely on pointwise nonlinearities do not predict induced motion opposite to the motion of the modulation envelope, (ii) although we know induced effects occur at motion discontinuities, the envelope (second-order) motion is uniform across the field, and (iii) there is no basis for a quantitative prediction of the speed of the induced motion. Explanations of the perception of second-order motion based on feature tracking (Seiffert & Cavanagh 1998; Derrington & Ukkonen 1999) would not naturally predict the speed or direction of the induced motion, since the features, if they can be identified, will travel with the contrast envelope.

Differences in the processing of first- and second-order motion sequences are frequently attributed to separate mechanisms when they could be more parsimoniously explained as stimulus-dependent variation in the performance of a single mechanism. Recently, neuropsychological evidence has been presented for a double

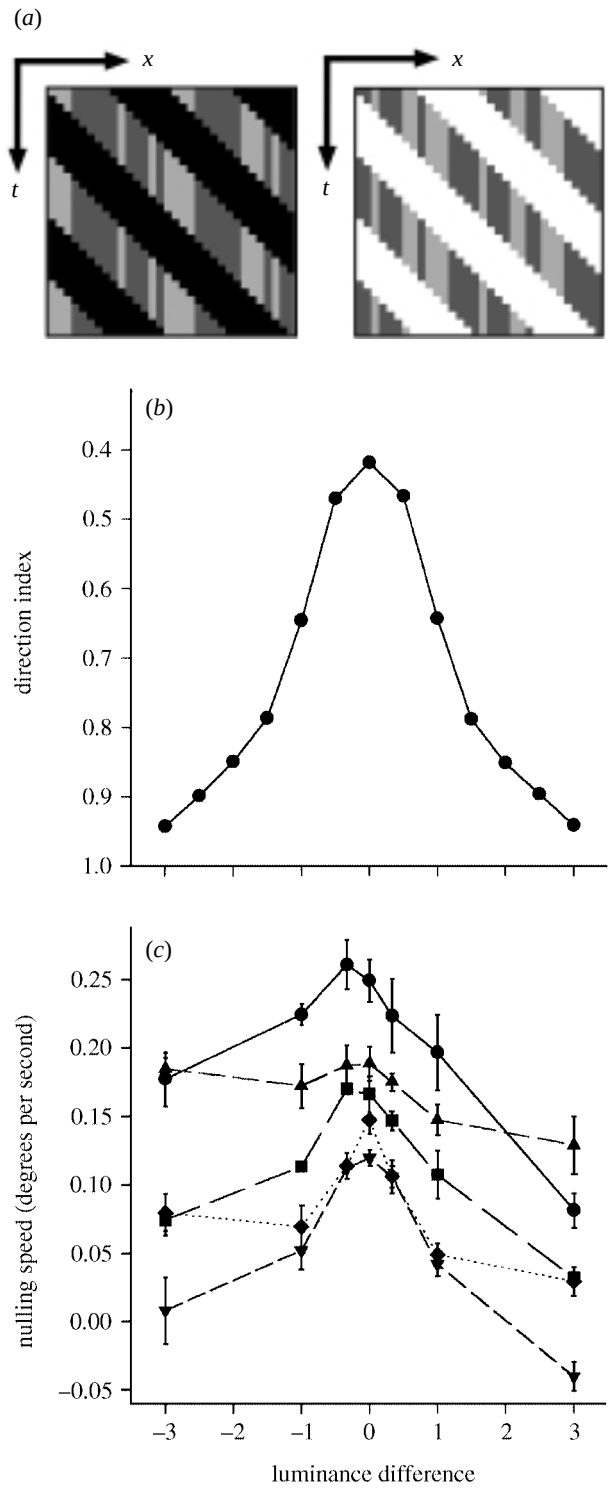

Figure 5. (*a*) Space–time plots showing examples of the motion stimuli at the extremes of the range investigated. (*b*) Model data showing the direction index as a function of the luminance difference as defined in § 6(a)(ii). (*c*) The size of the induced effect for square-wave modulation of contrast is shown as a function of the brightness of the grey regions in the texture-defined motion stimulus. Data for five subjects are shown: A.J. (circles), C.B. (squares), J.A. (triangles), J.D. (inverted triangles) and P.M. (diamonds).

dissociation of the processing of first- and second-order motion sequences (Vaina & Cowey 1996; Vaina *et al*. 1998) suggesting anatomically distinct regions for the analysis of first- and second-order motion. One patient, having a lesion close to human area V5–MT, showed impairment in tasks involving second-order motion but not first-order motion. Another patient with a lesion centred on putative areas V2 and V3 showed deficits in first-order motion tasks but not second-order tasks (see Clifford & Vaina (1999) for a detailed computer simulation). However, this result conflicts with neuropsychological evidence (Greenlee & Smith 1997) which found first- and second-order speed perception to be mediated by the same brain areas and functional imaging studies of areas active during the processing of first- and second-order motion sequences which showed similar locations activated for both kinds of stimuli (Smith *et al*. 1998; Somers *et al*. 1998). Smith *et al*. (1998) reported higher activation of human areas V3 and VP for second-order motion than first-order motion, which may indicate a specialism for second-order motion, but this is also counter to what would be expected from the Vaina *et al*. (1998) study. Neurons in areas 17 and 18 in cat cortex (Zhou & Baker 1993; Mareschal & Baker 1998) respond to both first- and second-order motion and recordings from area V5–MT (O'Keefe & Movshon 1998) in the primate indicate that neurons which respond to second-order motion (25% of the sample) also respond to first-order motion, although the response to second-order motion is generally weaker. Evidence for separate systems based on reports that optokinetic nystagmus is not driven by second-order motion (Harris & Smith 1992) has been undermined by the demonstration that adding dynamic noise to first-order motion also reduces optokinetic nystagmus (Cobo-Lewis *et al*. 1998). As yet anatomical, neurophysiological and neuropsychological studies have not provided unequivocal evidence of separate encoding of first- and second-order motion.

Ledgeway & Smith (1994) argued for separate channels after the observation that interleaved frames from first-order and second-order motion sequences do not give rise to the perception of a consistent direction of motion. However, this argument assumes that a mechanism which correctly signals direction for first-order and second-order sequences will also correctly signal direction in the interleaved case. Direct simulation using the model considered here shows this not to be the case (Benton *et al*. 1999). Weak cross-over of adaptation to first- and second-order motion (Nishida *et al*. 1997*b*) has also been offered as evidence of separate mechanisms. However, it is generally the case that adaptation is greatest for test patterns which are visually similar to adapting patterns. It is not clear whether the filters in a complex neural hierarchy activated and adapted by a first-order pattern are equally involved in the processing of particular second-order patterns and vice versa.

We have shown that a single computational strategy can predict the perceived speed and direction of motion in a range of texture-defined and flicker-defined motion sequences as well as for contrast-modulated sine-wave gratings (Johnston & Clifford 1995*a*). To detect texture-defined motion the neural computation must become insensitive to the sign of the luminance contrast. In a second-order channel the sign is forced to be positive by rectification and as such carries no information. In the gradient approach the signs of spatial and temporal derivatives are multiplied. The sign of this product

indicates the direction of motion irrespective of the sign of luminance contrast.

This work was supported by a project grant from the Biotechnology and Biological Sciences Research Council–Engineering and Physical Sciences Research Council Mathematical Modelling Initiative. We would like to thank Oliver Braddick for suggesting we might vary the bar luminance and Jason Dale for assistance with software development.

REFERENCES

Adelson, E. H. & Bergen, J. R. 1985 Spatiotemporal energy models for the perception of motion. *J. Opt. Soc. Am.* A **2**, 284–299.

Albright, T. 1992 Form-cue invariant motion processing in primate visual cortex. *Science* **255**, 1141–1143.

Badcock, D. R. & Derrington, A. M. 1989 Detecting the displacements of spatial beats: no role for distortion products. *Vision Res.* **29**, 731–739.

Benton, C. & Johnston, A. 1997 First-order motion from contrast modulated noise. *Vision Res.* **37**, 3073–3078.

Benton, C., McOwan, P. & Johnston, A. 1999 Computational modelling of interleaved first-order and second-order motion sequences and translating 3f + 4f beat pattern. *Perception* **28** (Suppl. 29).

Cavanagh, P. & Mather, G. 1989 Motion: the long and the short of it. *Spatial Vision* **4**, 103–129.

Chubb, C. & Sperling, G. 1988 Drift-balanced random dot stimuli: a general basis for studying non-Fourier motion perception. *J. Opt. Soc. Am.* A **5**, 1986–2007.

Clifford, C. W. G. & Vaina, L. M. 1999 A computational model of selective deficits in first and second-order motion processing. *Vision Res.* **39**, 113–130.

Cobo-Lewis, A. B., McCarron, A. R. & Tusa, R. J. 1998 Optokinetic nystagmus evoked by first- and second-order motion. *Invest. Ophthalmol. Vis. Sci.* **39**, S766.

Cropper, S. & Derrington, A. M. 1994 Motion of chromatic stimuli: first-order or second-order? *Vision Res.* **34**, 49–58.

Derrington, A. M. & Badcock, D. R. 1985 Separate detectors for simple and complex grating patterns? *Vision Res.* **25**, 1869–1878.

Derrington, A. M. & Ukkonen, O. I. 1999 Second-order motion discrimination by feature-tracking. *Vision Res.* **39**, 1465–1475.

Dunker, K. 1929 Uber induzierte Bewegung. In *Source book of Gestalt psychology* (ed. W. H. Ellis), pp. 161–172. New York: Routledge–Harcourt Brace.

Emerson, R. C., Bergen, J. R. & Adelson, E. H. 1992 Directionally selective complex cells and the computation of motion energy in cat visual cortex. *Vision Res.* **32**, 203–218.

Georgeson, M. A. & Shackleton, T. M. 1989 Monocular motion sensing, binocular motion perception. *Vision Res.* **29**, 1511–1523.

Greenlee, M. W. & Smith, A. T. 1997 Detection and discrimination of first- and second-order motion in patients with unilateral brain damage. *J. Neurosci.* **17**, 804–818.

Harris, L. R. & Smith, A. T. 1992 Motion defined exclusively by second-order characteristics does not evoke optokinetic nystagmus. *Vis. Neurosci.* **9**, 565–570.

Heeger, D. J. 1987 Model for the extraction of image flow. *J. Opt. Soc. Am.* A **4**, 1455–1471.

Johnston, A. & Clifford, C. W. G. 1995*a* Perceived motion of contrast modulated gratings: predictions of the multi-channel gradient model and the role of full-wave rectification. *Vision Res.* **35**, 1771–1783.

Johnston, A. & Clifford, C. W. G. 1995*b* A unified account of three apparent motion illusions. *Vision Res.* **35**, 1109–1123.

Johnston, A., McOwan, P. W. & Buxton, H. 1992 A computational model of the analysis of some first-order and second-order motion patterns by simple and complex cells. *Proc. R. Soc. Lond.* B **250**, 297–306.

Johnston, A., McOwan, P. W. & Benton, C. P. 1999 Robust velocity computation from a biologically motivated model of motion perception. *Proc. R. Soc. Lond.* B **266**, 509–518.

Ledgeway, T. & Smith, A. T. 1994 Evidence for separate mechanisms for first- and second-order motion in human vision. *Vision Res.* **34**, 2727–2740.

Ledgeway, T. & Smith, A. T. 1995 The perceived speed of second-order motion and its dependence on stimulus contrast. *Vision Res.* **35**, 1421–1434.

Lu, Z.-L. & Sperling, G. 1995*a* Attention-generated apparent motion. *Nature* **377**, 237–239.

Lu, Z.-L. & Sperling, G. 1995*b* The functional architecture of human visual motion perception. *Vision Res.* **35**, 2697–2722.

Mareschal, I. & Baker, C. L. 1998 A cortical locus for the processing of contrast-defined contours. *Nature Neurosci.* **1**, 150–154.

Nakayama, K. & Loomis, J. M. 1974 Optical velocity patterns, velocity sensitive neurones, and space perception: a hypothesis. *Perception* **3**, 63–80.

Nishida, S. & Sato, T. 1995 Motion after effect with flickering test patterns reveals higher stages of motion processing. *Vision Res.* **35**, 477–490.

Nishida, S., Edwards, M. & Sato, T. 1997*a* Simultaneous motion contrast across space: involvement of second order motion? *Vision Res.* **37**, 199–214.

Nishida, S., Ledgeway, T. & Edwards, M. 1997*b* Dual multiple scale processing for motion in the human visual system. *Vision Res.* **36**, 2685–2698.

Nowlan, S. J. & Sejnowski, T. J. 1994 Filter selection model for motion segmentation and velocity integration. *J. Opt. Soc. Am.* A **11**, 3177–3200.

O'Keefe, L. P. & Movshon, A. J. 1998 Processing of first- and second-order motion signals by neurones in area MT of the macaque monkey. *Vis. Neurosci.* **15**, 305–317.

Raymond, J. E. & Darcangelo, S. M. 1990 The effect of local luminance contrast on induced motion. *Vision Res.* **30**, 751–756.

Seiffert, A. E. & Cavanagh, P. 1998 Position displacement, not velocity, is the cue to motion detection of second-order stimuli. *Vision Res.* **38**, 3569–3582.

Simoncelli, E. P. & Heeger, D. J. 1998 A model of neuronal responses in visual area MT. *Vision Res.* **38**, 743–762.

Smith, A. T. & Scott-Samuel, N. E. 1998 Stereoscopic and contrast-defined motion. *Proc. R. Soc. Lond.* B **265**, 1573–1581.

Smith, A. T., Greenlee, M. W., Singh, K. D., Kraemer, F. M. & Hennig, J. 1998 The processing of first- and second-order motion in human visual cortex assessed by functional magnetic resonance imaging (fMRI). *J. Neurosci.* **18**, 3816–3830.

Solomon, J. A. & Sperling, G. 1994 Full-wave and half-wave rectification in second-order motion perception. *Vision Res.* **34**, 2239–2258.

Somers, D. C., Seiffert, A. E., Dale, A. M. & Tootell, R. B. H. 1998 Second-order motion stimulus-induced activation and attentional modulation of human visual cortical areas MT & V3a. *Invest. Ophthalmol. Vis. Sci.* **39**, 1129.

Vaina, L. M. & Cowey, A. 1996 Impairment of the perception of second order motion but not first order motion in a patient with unilateral focal brain damage. *Proc. R. Soc. Lond.* B **263**, 1225–1232.

Vaina, L. M., Makris, N., Kennedy, D. & Cowey, A. 1998 The selective impairment of the perception of first-order motion by unilateral cortical brain damage. *Vis. Neurosci*. **15**, 333–348.

Van Santen, J. P. H. & Sperling, G. 1985 Elaborated Reichardt detectors. *J. Opt. Soc. Am*. A**2**, 300–321.

Watson, A. B. & Ahumada, A. J. 1985 Model of human visual-motion sensing. *J. Opt. Soc. Am*. A **2**, 322–341.

Watt, R. J. & Andrews, D. P. 1981 APE: adaptive probit estimation of psychometric functions. *Curr. Psychol. Rev.* **1**, 205–214.

Werkhoven, P., Sperling, G. & Chubb, C. 1993 The dimensionality of texture-defined motion: a single channel theory. *Vision Res*. **33**, 463–485.

Wilson, H. R. & Kim, J. 1994 A model for motion coherence and transparency. *Vis. Neurosci*. **11**, 1205–1220.

Zanker, J. 1996 On the elementary mechanism underlying secondary motion processing. *Phil. Trans. R. Soc. Lond*. B **351**, 1725–1736.

Zhou, Y. & Baker, C. L. 1993 A processing stream in mammalian visual cortex neurones for non-Fourier responses. *Science* **261**, 98–101.

As this paper exceeds the maximum length normally permitted, the authors have agreed to contribute to production costs.